# Supporting Information

## Enhanced ordering in length polydisperse carbon nanotube solutions at high concentrations as revealed by small angle X-ray scattering

Vida Jamali, Francesca Mirri, Evan G. Biggers, Robert A. Pinnick, Lucy Liberman, Yachin Cohen, Yeshayahu Talmon, Fred C. MacKintosh, Paul van der Schoot, Matteo Pasquali*
*Email: mp@rice.edu, +1 (713) 348-5830

## 2D SAXS plots for CNT-CSA solutions

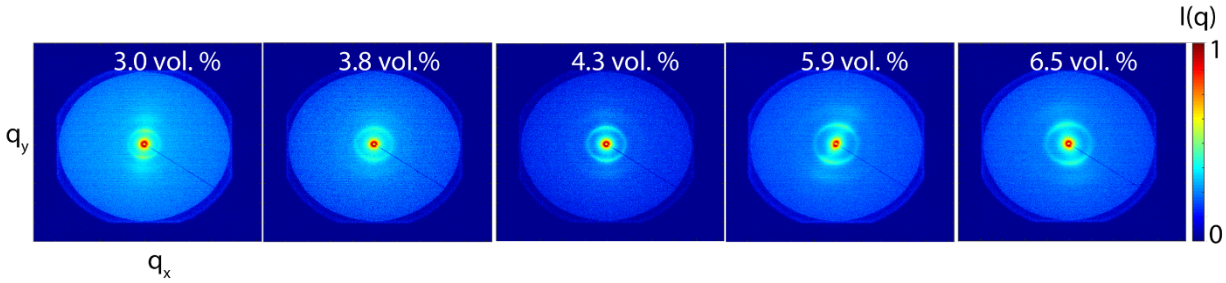


**Figure S1. 2D SAXS plots for CNT-CSA solutions in concentration ranging from 3 to 6.5 % by volume.**

Figure S1 shows the plots of 2D SAXS data for CNT-CSA solutions at concentrations of 3, 3.8. 4.3, 5.9, and 6.5 % by volume. These volume fractions correspond to 2.2, 2.8, 3.2, 4.4, and 4.8 % by weight, respectively (The density of CSA is 1.73 g/cm$^3$ and the density of the CNT is about 1.3 g/cm$^3$ as reported in the Materials and Methods section). Most of the samples show an azimuthally anisotropic 2D pattern due to the overall alignment of the liquid crystal solution along the long axis of the capillary tube. This preferential alignment might be related to the loading process that applies a shear to the solution and the long relaxation time for the highly viscous solutions of CNT in CSA at high concentrations. The capillary tubes were allowed to rest overnight before testing to let the samples get to their equilibrium condition.

# Analysis of the SAXS data from CNT-CSA solutions

The emergence of peaks in the $I(q)$ *vs*. $q$ curve shows a certain type of ordering in the solution. In order to extract more information about this ordering an its nature, we need to find the peak positions and relate them to the real-space distances in the solution using Bragg's law. All the data analysis and fittings here was done using the Irena and Nika macro suite [1, 2] within the Igor Pro software (Wavemetrics, Lake Oswego, OR) as described below.

For plotting the 1D $I(q)$ *vs*. $q$ curve, the 2D data must be integrated azimuthally to obtain the 1D data. Here, our 2D signals are anisotropic and hence we integrated the signal only over the anisotropy angle, i.e., the alignment direction that is along the long axis of the capillary tube (e.g., $\sim 90^\circ \pm 5$ and $\sim 180^\circ \pm 5$). The azimuthally-averaged scattering signal is the sum of various contributions including the signal form the local ordering of CNT particles, CSA solvent, and the glass capillary tube. To find the contribution form the glass wall and the CSA solvent, a glass capillary tube filled with the solvent was tested separately for 1 hour and subtracted from the data for each individual concentration. The scattering signal was then normalized and presented as $I(q)$ vs. $q$ curve in Figure 3.

The $I(q)$ signals exhibit two main features: and apparent power-law scattering at low $q$ and three diffraction peaks at higher $q$, above a flat background , $I_{BG}$ (Eq. S1).

$$I(q) = I_{BG} + Bq^{-n} + \sum_{peaks} K_i f_i(q), \qquad \text{(S1)}$$

Here, $K_i$ is the scaling factor for each diffraction peak. Each peak is modeled as a Lorentzian function $f(q) = M\frac{\Lambda}{\pi(\Gamma^2+(q-\mu)^2)}$, with $M$ the scaling factor, $\Lambda$ the Lorentzian width, and $\mu$ the center of the peak. The power-law is given by the exponent $n$ and prefactor $B$. The Levenberg-Marquardt least-square algorithm was used for fitting and parameter optimization[1]. Here, we fitted a hexagonally-close-packed (HCP) cylinder model (for a hexagonally packed columnar phase with $q_2/q_1 = \sqrt{3}$) to our data on concentrations 3-6.5 % by volume. Table S1 presents our fitting parameters for all the concentrations tested. The fitted power law exponents are close to the value

given by Porod's law ($n = -4$). This may be due to the surface of large structures, such as boundaries of liquid crystalline domains, the dimensions of which are larger than the inverse of the smallest accessible $q$.

**Table S1. Fitting parameters of a hexagonally close-packed cylinder model for concentrations ranging from 3 to 6.5 % by volume.**

| | **Concentration (% by volume)** | | | | |
|---|---|---|---|---|---|
| **Fitting Parameters** | **3** | **3.8** | **4.3** | **5.9** | **6.5** |
| $B$ | $3.1 \times 10^{-11}$ | $6.3 \times 10^{-11}$ | $1.2 \times 10^{-11}$ | $1.5 \times 10^{-10}$ | $2.3 \times 10^{-11}$ |
| $n$ | 3.92 | 3.71 | 4.17 | 4.04 | 3.83 |
| Background | $1.1 \times 10^{-3}$ | $1.8 \times 10^{-3}$ | $9.6 \times 10^{-4}$ | $9.2 \times 10^{-4}$ | $8.8 \times 10^{-4}$ |
| Peak 1 position | 0.052 | 0.060 | 0.061 | 0.071 | 0.075 |
| Peak 1 width | 0.007 | 0.009 | 0.006 | 0.009 | 0.009 |
| Peak 1 Prefactor | 4358 | 5811 | 7266 | 1501 | $1.7 \times 10^{4}$ |
| Peak 2 width | 0.019 | 0.026 | 0.021 | 0.025 | 0.033 |
| Peak 2 Prefactor | 4902 | 7378 | 7197 | 1331 | $1.1 \times 10^{4}$ |
| Peak 3 width | 0.017 | 0.015 | 0.014 | 0.019 | 0.023 |
| Peak 3 Prefactor | 5362 | 6409 | 9425 | 1356 | $1.2 \times 10^{4}$ |

In order to verify whether the second scattering peak is related to the first form factor peak of CNT as cylindrical objects, we plotted the form factor, $F(q)$, for our CNT system with diameter $D \approx 2$ nm (Eq. S2)[3]. The highlighted area in pink shows the $q$ range probed using SAXS in this study (Figure S2). The first form factor peak is located at $q^*$~0.5 $A^{-1}$, outside the range probed by the SAXS (0.0075 to 0.25 $A^{-1}$). Therefore, we can assure that the second peak is not associated with the form factor peaks of cylindrical particles in the system.

$$F(q) \propto \left(\frac{J_1(qR)}{qR}\right)^2 \tag{S2}$$

Here, $J_1$ is the first-order Bessel function and $R$ is the average radius of CNTs.

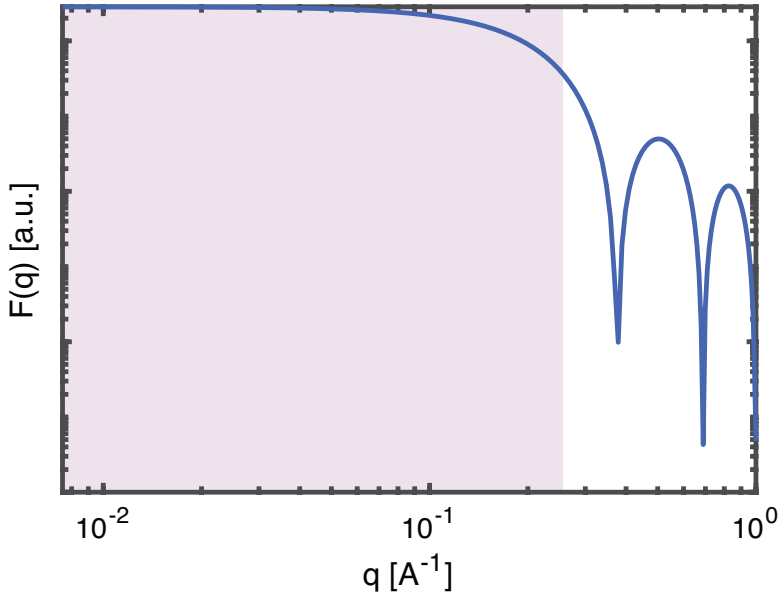


**Figure S2. Form factor of cylinders of diameter $D \approx 2$ nm. The highlighted area shows the q range probed using SAXS in this work.**

The second possibility for the presence of the interference peaks is the liquid-like structure in hard-rod solutions that can occur below the nematic-columnar transition point. The relative position of these peaks will not change by changing the volume fraction of the rods in solution as long as the concentration remains below the nematic-columnar transition point. However, the intensity of these peaks is quite sensitive to the concentration of the scattering particles in solution[3].

In order to find the structure factor, $S(q)$, of a polydisperse rod-like system, we first calculate the direct correlation function $c_{ij}(\boldsymbol{r})$, describing the short-range interactions between two rods of length $L_i$ and $L_j$. We can use second virial approximation for low volume fractions (below the nematic-columnar transition point) to calculate the direct correlation function, $c_{ij}(\boldsymbol{r}) = \Gamma f_{ij}(\boldsymbol{r})$, where $f_{ij}(\boldsymbol{r})$ is the Mayer function and $f_{ij}(\boldsymbol{r}) = \exp\left(-\frac{U_{ij}(\boldsymbol{r})}{k_B T}\right) - 1$.[4] with $U_{ij}(\boldsymbol{r})$ the pair-wise interaction potential, $T$ the temperature, and $k_B$ the Boltzmann constant. Based on the Lee-Parson's approximation, $\Gamma$ is a factor that accounts for higher body interactions in hard-rod liquid and is defined as $\Gamma = (1 - \frac{3\Phi}{4})/(1 - \Phi')^2$, where $\Phi'$ is the effective volume fraction of the rods in the solution[4, 5]. For the case of CNT-CSA solution, we can assume that CNT rod-like particles with effective diameter $D'$ (accounting for the Debye screening length and the mean amplitude of the thermal undulations), interact via a hard core excluded volume potential $U(\boldsymbol{r})$:

$$U(\boldsymbol{r}) = \begin{cases} \infty & \boldsymbol{r} < D' \\ 0 & \boldsymbol{r} > D' \end{cases} \tag{S3}$$

For simplicity, we can assume rods are parallel to each other as is the case for hard-rod solutions in nematic phase and only consider the structural ordering in the lateral plane. This is consistent with the fact that for sufficiently length-polydisperse system of rods, a direct nematic-columnar transition is expected to happen at high concentrations and the formation of smectic phase is suppressed; hence, there would be no positional ordering in the axial direction.[6] Therefore, we set $q_{||} = 0$ and only study the structure factor in the $q_\perp$ plane. We can then write the structure factor as a function of the direct correlation function as follows:[3, 5]

$$S(q_\perp) = \frac{1}{1 - n\langle\langle \hat{c}_{ij}(q_\perp)\rangle\rangle}, \tag{S4}$$

where $\langle\langle \hat{c}_{ij}(q_\perp)\rangle\rangle = \sum_i x_i \sum_j x_j \ \hat{c}_{ij}(q_\perp)$ denotes an average over the length distribution $x_i$, $\hat{c}_{ij}(q_\perp)$ is the spatial Fourier transform of $c_{ij}(r)$, and $n$ is the number density of the particles in solution. The solution to this equation is:

$$S(q_\perp) = \frac{1}{1 + 16\phi'\Gamma \int_0^1 t J_0(q_\perp D' t)\mathrm{d}t}, \tag{S5}$$

with $J_0$, the Bessel of function of the first kind of order zero.

Here, we plotted the structure factor $S(q_\perp)$, which is directly proportional to the scattering intensity $I(q)$, for different concentrations below the nematic-columnar transition point. Figure S3a shows that regardless of the volume fraction, the relative position of the second peak with respect to the first peak is about $\sqrt{5}$.[3] Using the form factor of cylinders $F(q)$, described in the previous section (eq. S2) and the obtained structure factor $S(q)$, we can then reconstruct $I(q) \propto S(q)F(q)$ as shown in Figure S3b. The discrepancy between the position of the second peak in the experimental data (for the lowest concentration tested, i.e., 3% by volume) compared to the model intensity with peaks positioned at $1:\sqrt{5}:\sqrt{12}$ (Figure S3c), confirms that the higher order peaks in our data are not associated with the interference peaks from hard-rod nematic liquid or neither the form factor of the rod-like particles.

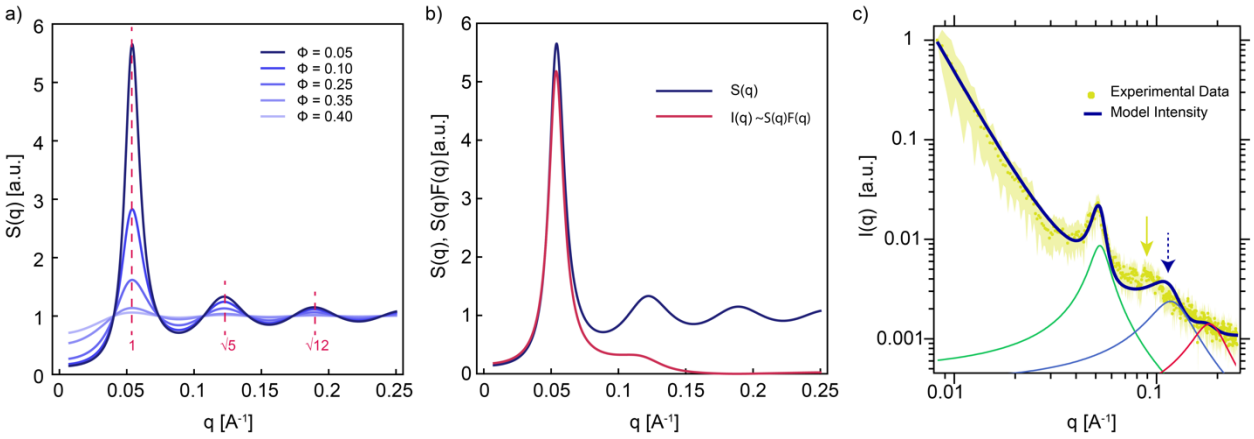


**Figure S3. a) Structure factor $S(q_\perp)$ vs. momentum transfer $q_\perp$, in the radial plane for a hard-rod liquid at various volume fractions, $\phi'$, below the nematic-columnar transition point showing that the relative spacing of the peaks remains constant upon increasing the concertation (relative peak position of $1:\sqrt{5}:\sqrt{12}$). b) Structure factor $S(q_\perp)$ and $I(q_\perp) \propto S(q_\perp)F(q_\perp)$ calculated for $\phi' = 0.4$ showing the position of the interference peaks remains almost unchanged. c) Scattering intensity of the lowest concentration (3% by volume) studied in this work compared to a model intensity curve constructed using the model described in eq. S1 but with interference peaks positioned at $1:\sqrt{5}:\sqrt{12}$ representing a hard-rod liquid. Arrows indicate the position of the second peak in the experimental scattering data (solid) and the model intensity (dashed).**

## Raman peak shift for dry CNTs vs. CNT in solution

The degree of protonation was quantified by measuring the upshift in the G peak of the Raman spectra. This shift is independent of the CNT concentration, and can be correlated to the fractional positive charge per carbon atoms [7, 8]. Previous studies have shown that quenching the acid restores the G-peak position and that no D-band appears in the spectrum, indicating that protonation by CSA does not damage the CNTs, and is fully reversible [9].

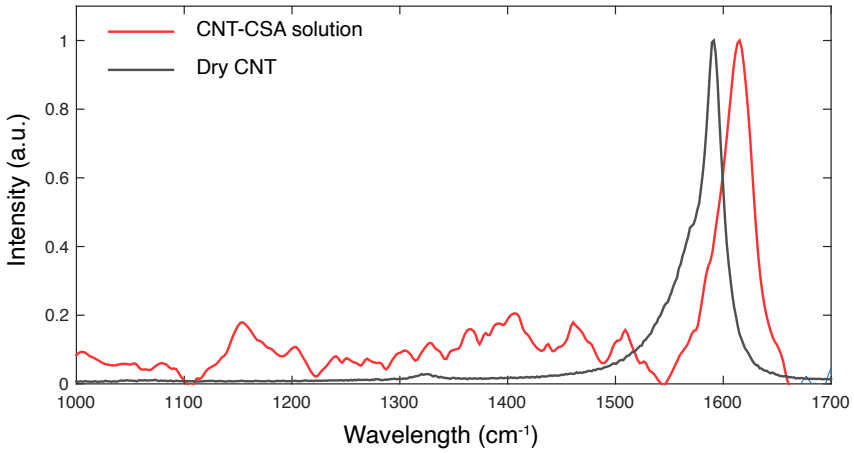


**Figure S4. $E_{2g}$ peak of the Raman spectra for CNTs before dissolution in CSA (black) vs. CNTs dissolved in CSA (red). The $E_{2g}$ peak is at 1591.3 $cm^{-1}$ for the CNTs before the dissolution, and 1615.1 $cm^{-1}$ for the CNTs in solution, which corresponds to a shift of 23.8 $cm^{-1}$.**

**References:**


1. Ilavsky, J.; Jemian, P. R., Irena: tool suite for modeling and analysis of small-angle scattering. *Journal of Applied Crystallography* **2009,** *42*, 347-353.
2. Ilavsky, J., Nika: software for two-dimensional data reduction. *Journal of Applied Crystallography* **2012,** *45*, 324-328.
3. Cohen, Y.; Thomas, E. L., On the modeling of small-angle X-ray-scattering from systems of oriented fibrils. *Journal of Polymer Science Part B-Polymer Physics* **1987,** *25* (8), 1607-1614.
4. van der Schoot, P., The nematic-smectic transition in suspensions of slightly flexible hard rods. *Journal De Physique Ii* **1996,** *6* (11), 1557-1569.
5. Hansen, J.-P.; McDonald, I. R., *Theory of simple liquids: with applications to soft matter*. Academic Press: 2013.

6. Bohle, A. M.; Holyst, R.; Vilgis, T., Polydispersity and ordered phases in solutions of rodlike macromolecules. *Physical Review Letters* **1996,** *76* (8), 1396-1399.
7. Ramesh, S.; Ericson, L. M.; Davis, V. A.; Saini, R. K.; Kittrell, C.; Pasquali, M.; Billups, W. E.; Adams, W. W.; Hauge, R. H.; Smalley, R. E., Dissolution of pristine single walled carbon nanotubes in superacids by direct protonation. *Journal of Physical Chemistry B* **2004,** *108* (26), 8794-8798.
8. Puech, P.; Hu, T.; Sapelkin, A.; Gerber, I.; Tishkova, V.; Pavlenko, E.; Levine, B.; Flahaut, E.; Bacsa, W., Charge transfer between carbon nanotubes and sulfuric acid as determined by Raman spectroscopy. *Physical Review B* **2012,** *85* (20), 205412.
9. Davis, V. A.; Parra-Vasquez, A. N. G.; Green, M. J.; Rai, P. K.; Behabtu, N.; Prieto, V.; Booker, R. D.; Schmidt, J.; Kesselman, E.; Zhou, W.; Fan, H.; Adams, W. W.; Hauge, R. H.; Fischer, J. E.; Cohen, Y.; Talmon, Y.; Smalley, R. E.; Pasquali, M., True Solutions of Single-Walled Carbon Nanotubes for Assembly into Macroscopic Materials. *Nature Nanotechnology* **2009,** *4* (12), 830-834.